Kinetic Study of the Gas-Phase Reaction of OH with Br_2

Mikhail G. Bryukov and Barry Dellinger*

Department of Chemistry, Louisiana State University, Baton Rouge, Louisiana 70803

Vadim D. Knyazev

Research Center for Chemical Kinetics, Department of Chemistry, The Catholic University of America, Washington, D.C. 20064

Received: February 17, 2006; In Final Form: May 22, 2006

An experimental, temperature-dependent kinetic study of the gas-phase reaction of the hydroxyl radical with molecular bromine (reaction 1) has been performed by using a pulsed laser photolysis/pulsed-laser-induced fluorescence technique over a wide temperature range of 297−766 K, and at pressures between 6.68 and 40.29 kPa of helium. The experimental rate coefficients for reaction 1 demonstrate no correlation with pressure and exhibit a negative temperature dependence with a slight negative curvature in the Arrhenius plot. A nonlinear least-squares fit with two floating parameters of the temperature-dependent $k_1(T)$ data set using an equation of the form $k_1(T) = AT^n$ yields the recommended expression $k_1(T) = (1.85 \times 10^{-9})T^{-0.66}$ cm^3 molecule^{-1} s^{-1} for the temperature dependence of the reaction 1 rate coefficient. The potential energy surface (PES) of reaction 1 was investigated with use of quantum chemistry methods. The reaction proceeds through formation of a weakly bound OH···Br_2 complex and a PES saddle point with an energy below that of the reactants. Temperature dependence of the reaction rate coefficient was modeled by using the RRKM method on the basis of the calculated PES.

I. Introduction

Brominated flame retardants are widely used chemicals, and over the years, more and more materials containing brominated organics are being subjected to thermal degradation in hazardous and municipal waste incinerators or accidental fires.[1] Brominated flame retardants are useful but also potentially damaging to the environment. They are frequently burned in the presence of chlorinated materials and upon combustion or thermal degradation can form various brominated/chlorinated byproducts including polybrominated/chlorinated dibenzo-*p*-dioxins and dibenzofurans (PBCDD/F).[1−4] Their properties are similar to PCDD/Fs that are classified as carcinogenic and known to cause birth defects and chloroacne. This has stimulated the development of research directed at mechanistic and chemical kinetic modeling of combustion of bromo-chloro-organics. Accurate chemical kinetic modeling is essential for understanding the complicated chemistry of these processes.

Along with the reactions of the hydroxyl radical with HCl, Cl_2, and HBr, the gas-phase reaction of the hydroxyl radical with molecular bromine

$$OH + Br_2 \rightarrow \text{products} \qquad (1)$$

probably plays a significant role in the combustion chemistry of bromo-chloro-organics. In the post-flame zone it should deplete OH and thus inhibits CO oxidation. Via this reaction, Br_2 molecules are converted to Br atoms that should have a significant effect on the concentration of brominating and chlorinating agents including BrCl that controls the composition of the final emissions of the polybromo-chloro-aromatic pollutants.[1−4] Although reaction 1 is potentially important in these processes, the rate coefficient of this reaction has not been studied at high temperatures.

To our knowledge, the kinetics of reaction 1 has been directly investigated in five studies[5−9] performed at low temperatures only. The importance of this reaction for atmospheric chemistry is described, e.g., in the earlier studies of Gilles et al.[8] and Bedjanian et al.[9] The current work represents the first experimental study of reaction 1 carried out at high temperatures in the range from 297 K (to compare with the earlier studies) to 766 K, which is relevant to combustion and other thermal processes.

II. Experimental Section

II.A. Experimental Technique. The experimental study of the temperature dependence of the rate coefficient for the reaction of the hydroxyl radical with molecular bromine was performed with a pulsed laser photolysis/pulsed-laser-induced fluorescence (PLP/PLIF) technique combined with a heatable, slow-flow reactor under pseudo-first-order conditions with a large excess of molecular bromine. The experimental setup has been described in detail in our previous article[10] and is considered here only briefly.

An excimer laser and an Nd:Yag pumped, frequency doubled, tunable pulsed dye laser were employed to generate the photolysis and probe laser pulses, respectively. Hydroxyl radicals were formed by the 193-nm pulsed laser photolysis of N_2O to $O(^1D)$ and N_2, and the subsequent rapid reaction of $O(^1D)$ with H_2O.[11,12]

$$N_2O + h\nu(193\text{ nm}) \rightarrow N_2 + O(^1D) \qquad (2)$$

$$O(^1D) + H_2O \rightarrow 2OH \qquad (3)$$

* To whom correspondence should be addressed. E-mail: barryd@lsu.edu.

10.1021/jp061038m CCC: $33.50 © 2006 American Chemical Society
Published on Web 06/29/2006

OH was excited by the probe laser pulse at ~282 nm via the $A^2\Sigma^+ - X^2\Pi$ (1−0) transition followed by observation of fluorescence from the (1−1) and (0−0) bands at 308−316 nm (see, for example, refs 13 and 14). The fluorescent radiation was monitored with a photomultiplier tube, using a UV band-pass filter (308 nm peak transmission) to minimize scattered light. The signal from the photomultiplier was amplified and then recorded by a 500-MHz digital oscilloscope to obtain the integrated voltage averaged for a desired number of laser pulses (typically 50−150) at a single time delay. The value, S_t, received from the integration of the average voltage signal is a sum of two components: the integral from the average LIF signal of OH radicals, S_{OH} (this term is proportional to the absolute concentration of OH), and the integral from the average scattered light signal, S_{sc}. The average integrated voltage for the scattered light was measured directly in the absence of OH radicals. For this measurement, the photolysis laser was not triggered during the accumulation of the scattered light signal. Kinetic information was obtained by varying the time delay between pulses of the photolysis and the probe lasers in the desired time interval by using a digital delay generator.

We utilized four individually controlled flows of He (main carrier gas flow), H_2O/He, N_2O/He, and Br_2/Ar to prepare a reaction gas mixture. Three calibrated mass-flow controllers with appropriate flow ranges were employed to set the values of the three gas flows of He (main carrier gas flow), H_2O/He, and N_2O/He and maintain their stability during the performance of the experiments. At selected times during the experiments, values of these three flows were controlled by measuring rates of pressure increases in the calibrated volumes located upstream from the gas inlet of the reactor. The fourth flow of Br_2/Ar was manually regulated by a metering valve. This flow was also determined by measuring the rate of the pressure increase in the calibrated volume before and after obtaining each OH temporal profile. A mean value of these two flow measurements was taken to calculate Br_2 concentration in the reaction zone. These pressure measurements were performed with capacitance manometers of 100.00 and 1000.0 Torr ranges (1 Torr = 133.322 Pa).

The independence of the measured flows on the surface-to-volume ratio of the calibrated volume was verified to ensure the absence of interference from heterogeneous absorption and desorption processes on the walls of the volume by using three different calibrated Pyrex vessels (150.2, 724.5, and 6364 cm^3). Bromine was accurately, manometrically diluted with argon in a Pyrex vacuum system and stored in a ~22 L Pyrex bulb and a ~9 L Pyrex cylindrical reservoir (~13.5 cm i.d. × ~68 cm length). These two reservoirs with different surface-to-volume ratios were used with the expressed purpose of verifying the absence of interference from Br_2 heterogeneous absorption and desorption processes on the walls of the containers. To minimize systematic error in the Br_2 concentration determination, we had prepared four Br_2/Ar mixtures with different concentrations of Br_2 ranging between 1.433% and 4.97%, and these were used without any correlation between Br_2 concentrations in those and established reaction temperatures.

All flows were premixed and directed though the pressure, temperature controlled, resistively heatable quartz reactor. The composite flow conditioned the reactor for several minutes prior to data collection, thereby minimizing any effects due to reactant adsorption on the delivery system and reactor walls, thus stabilizing the established experimental conditions. The total flow rate ranged between 8.7 and 25.5 STP $cm^3\ s^{-1}$. The total pressure in the reactor was measured with the capacitance manometers of 100.00 and 1000.0 Torr ranges. The gas temperature in the reaction zone was monitored with a retractable Chromel-Alumel thermocouple. The maximum total uncertainty in the measurements of the reaction temperatures, T, did not exceed 0.5% of T. (See ref 10 for details.)

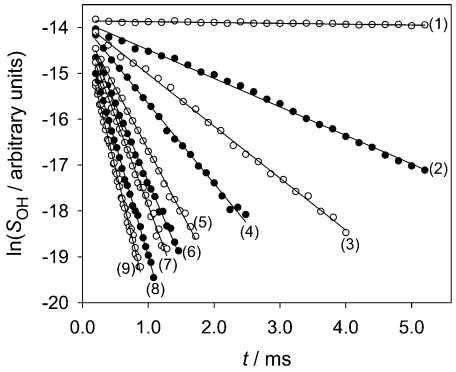

Figure 1. Examples of relative OH concentration temporal profiles obtained under the following conditions: helium buffer gas, temperature $T = 766$ K, total pressure $P = 40.29$ kPa (302.2 Torr), $[N_2O] = 3.17 \times 10^{13}$ molecule cm^{-3}, $[H_2O] = 1.8 \times 10^{15}$ molecule cm^{-3}; $[Br_2] = 0$, 3.07×10^{13}, 5.79×10^{13}, 8.11×10^{13}, 1.22×10^{14}, 1.52×10^{14}, 1.76×10^{14}, 2.28×10^{14}, and 2.64×10^{14} molecule cm^{-3} for profiles 1−9, respectively.

The molecular concentration of each reagent in the reaction zone was derived from its partial concentration, measurements of the flow rates, the reaction temperature, and total pressure under the ideal gas assumption. Typical reaction mixtures used in these experiments consisted of the following molecular concentration ranges (units of molecule cm^{-3}): N_2O, 2.02×10^{13} to 7.11×10^{13}; H_2O, 1.0×10^{15} to 2.0×10^{15}; He, 1.51×10^{18} to 3.81×10^{18}; Ar, 0.0 to 1.08×10^{16}; Br_2, 0.0 to 2.64×10^{14}.

The chemicals utilized in this study had the following stated minimum purities (supplier): He, 99.999% (The BOC Group, Inc.); Ar, 99.999% (The BOC Group, Inc.); Br_2, 99.99% (Aldrich); N_2O, 9.98% mixture of 99.99% purity in 99.999% He (The BOC Group, Inc.); and H_2O, A.C.S. reagent grade (Sigma-Aldrich). Analysis of the Br_2 sample showed only very small levels of impurities, and these very small concentrations had a negligible effect on the observed OH decay rates.

II.B. Reaction Rate Measurements and Results. All kinetics runs were performed under pseudo-first-order conditions in a large excess of molecular bromine with respect to the initial concentration of the hydroxyl radical, $[OH]_0$, which ranged approximately from 1.0×10^{10} to 1.9×10^{11} molecule cm^{-3}. The initial concentrations of OH radicals were estimated by a procedure similar to that described in ref 10. An uncertainty in the ratio between any two values of $[OH]_0$ taken at the same temperature is about 10%. Exact knowledge of the initial OH concentrations is not critical for determination of rate coefficients because the experiments were carried out under pseudo-first-order conditions with a large excess of bromine. The evaluated detection sensitivity limit for OH radicals, defined by unity signal-to-noise ratio, was around 1×10^8 molecule cm^{-3}.

A typical set of OH temporal profiles (a set of experiments) are presented in Figure 1 as a plot of $\ln(S_{OH}) = \ln(S_t - S_{sc})$ versus time delays, t. The initial detection time, t_0, for each set of experiments was established depending on experimental conditions, so that this time delay followed the photolysis of the reaction mixture and was sufficient for the completion of the reaction $O(^1D)$ with H_2O and for rotational and vibrational equilibration of OH radicals to the Boltzmann distribution.[12,15]

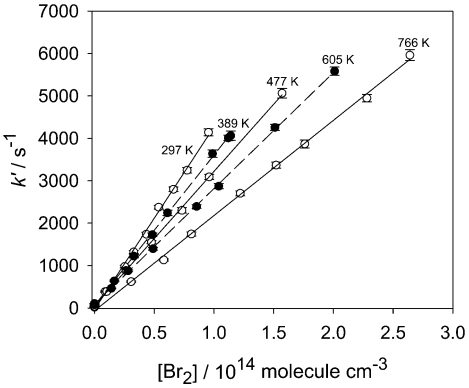

Figure 2. Examples of experimentally obtained k' vs $[Br_2]$ dependencies.

The initial detection time value, t_0, in all OH temporal decay profiles was not less than 0.2 ms (vide infra).

OH radical temporal profiles were analyzed by assuming the pseudo-first-order kinetic behavior of the OH signal:

$$\ln(S_{OH}) = \ln(S_t - S_{sc}) = \text{constant} - k't \qquad \text{(I)}$$

where the effective first-order rate coefficient, k', is given by

$$k' = k_1[Br_2] + k_0 \qquad \text{(II)}$$

k_1 is the bimolecular rate coefficient for reaction 1; $[Br_2]$ is the molecular bromine concentration; k_0 is the effective first-order rate coefficient of OH decay due to possible OH reactions with background impurities in the buffer gas, N_2O, H_2O, and OH diffusion/flow out of the detection zone (OH background loss). The effective first-order rate coefficient values, k', were obtained from linear least-squares fits of the experimental values $\ln(S_{OH})$ to eq I. (These least-squares fits and all next least-squares fits were performed with no weighting of the data points.)

Examples of measured k' versus bromine concentration dependences are presented in Figure 2. We determined the bimolecular rate coefficient, k_1, from the slope of the least-squares straight line through the k' versus $[Br_2]$ data points including the $(0, k_0)$ point, where k_0 was derived from the OH temporal profile directly measured at zero concentration of Br_2. For each set of experiments, the difference between the value of k_0 directly measured in the absence of bromine and k_0 found from the zero-abscissa intercept of the least-squares straight line in the ($[Br_2]$, k') coordinates was within the experimental uncertainties (2σ level of statistical uncertainties obtained from the linear least-squares fits). We analyzed the possible effect of a minor deviation from the first-order kinetic behavior of the OH background loss on the measurement of k_1 values using data processing with the background-loss correction described in refs 10 and 16−19. Under all the experimental conditions in our study, it was found that this effect was very small (less than 0.8% of the k_1 value) such that no background-loss correction was necessary.

The kinetic study of the reaction OH with molecular bromine was performed over the temperature range 297−766 K and at pressures between 6.68 and 40.29 kPa of helium. The experimental conditions and bimolecular rate coefficients measured for reaction 1 are summarized in Table 1. Over the entire experimental temperature range, the initial concentration of the hydroxyl radicals was varied by changing the photolysis laser intensity and the concentration of N_2O from set to set of experiments.

TABLE 1: Conditions and Results of Experiments To Measure Rate Coefficients of the Reaction of Hydroxyl Radicals with Molecular Bromine

no.[a]	T/K	P/kPa	$[Br_2]$ range/10^{12} molecule cm^{-3}	I[b]/mJ pulse^{-1} cm^{-2}	$[OH]_0/10^{10}$ molecule cm^{-3}	k_1[c]$/10^{-11}$ molecule^{-1} cm^3 s^{-1}
1	297	13.41	8.89−95.4	13	12	4.30 ± 0.17
2	321	6.68	14.1−108	7.2	5.1	4.226 ± 0.059
3	321	6.68	14.4−109	1.4	1.0	4.143 ± 0.072
4	349	13.41	7.32−88.9	16	7.1	3.75 ± 0.16
5	349	13.41	7.33−89.2	4.5	2.0	3.81 ± 0.17
6	389	13.41	16.6−114	13	4.8	3.546 ± 0.073
7	389	13.41	16.8−115	12	4.4	3.50 ± 0.18
8	477	13.41	10.27−128	12	19	3.167 ± 0.060
9	477	13.41	10.34−128	2.8	4.4	3.190 ± 0.097
10	541	26.88	5.50−156	6.0	3.7	2.927 ± 0.090
11	541	26.88	5.81−157	8.6	5.3	2.974 ± 0.094
12	605	13.40	14.1−201	11	18	2.734 ± 0.039
13	605	13.40	14.2−197	1.6	2.6	2.721 ± 0.049
14	686	26.88	10.1−170	11	2.7	2.45 ± 0.11
15	686	26.88	10.3−163	11	15	2.50 ± 0.14
16	765	13.40	9.36−246	16	18	2.283 ± 0.054
17	765	13.40	10.0−248	2.8	3.2	2.34 ± 0.12
18	766	40.29	30.7−264	12	19	2.245 ± 0.060

[a] Experiment number. [b] Photolysis laser intensity. [c] Error limits represent 2σ statistical uncertainties only. Maximum estimated systematic uncertainty is 5% of the rate coefficient value (see text).

The measured rate coefficients demonstrate no correlation with pressure or initial concentration of hydroxyl radicals within the experimental ranges. The independence of the rate coefficient values on the initial OH radical concentration indicates the absence of any effect of possible secondary reaction on the behavior of the kinetics of OH radical decay, that should be due to the low values of $[OH]_0 \approx (1.0-19) \times 10^{10}$ molecule cm^{-3}. Similarly, the observed absence of any correlation between the measured rate coefficients and the photolysis laser intensity shows that the potential effects of reactions of OH with the products of the photolysis of molecular bromine are negligible. At the highest reaction temperatures established in this study, the absence of any potential effects from thermal decomposition of molecular bromine was verified by measuring rate coefficients at different pressures and bulk flow velocities varied by factors of approximately 3 and 2, respectively.

In all experiments water was added to the reaction mixtures and its concentration was varied from 1.0×10^{15} to 2.0×10^{15} molecule cm^{-3} from set to set of experiments to ensure that the reaction of $O(^1D)$ with H_2O, and rotational and vibrational equilibration of OH radicals to the Boltzmann distribution proceeded sufficiently fast and had negligible effect on the measured rate coefficients (see refs 12 and 15, respectively). Furthermore, over the entire experimental temperature range, we selectively obtained temporal profiles of the formation of $OH(\nu=0)$ under typical experimental conditions in the absence of molecular bromine. We observed a prompt $OH(\nu=0)$ formation, which was always much faster than t_0, indicating that the reaction of $O(^1D)$ with H_2O, and rotational and vibrational equilibration of OH radicals to the Boltzmann distribution proceeded fast enough to be neglected at the time delays $t \geq t_0$. Otherwise, a nonprompt $OH(\nu=0)$ formation would be observed due to the lack of completion of these processes.

Figure 3 displays an Arrhenius plot of our $k_1(T)$ data along with those from previous studies. (Plotted error bars for our data and the data from ref 8 were calculated by taking the square root of the sum of the squares of the statistical and systematic errors.) The experimental variation of the reaction 1 rate coefficients with temperature obtained in the current study

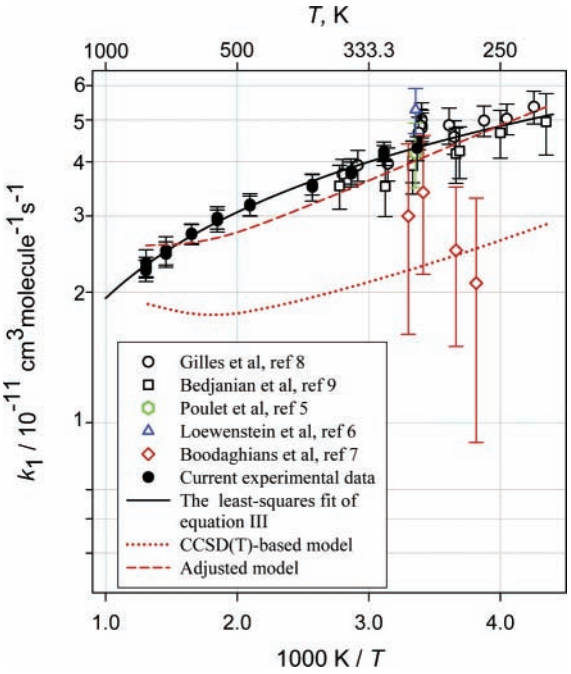

Figure 3. Temperature dependence of the rate coefficient for the reaction of OH with Br_2 displayed in Arrhenius coordinates. Open green hexagon, blue triangle up, red diamonds, black circles, squares, and filled black circles represent experimental data from refs 5−9 and current experimental data, respectively. The black solid line represents the least-squares fit of eq III (see text). The dotted and the dashed red lines represent the results of computational modeling of reaction 1 performed in the current study. The dotted red line is the model based on CCSD(T)/aug-cc-pVTZ//CCSD/aug-cc-pVDZ calculations; the dashed red line is the model with the PES saddle point energy decreased by 2.0 kJ mol^{-1}.

exhibits a negative temperature dependence with a slight negative curvature in the Arrhenius coordinates. A nonlinear least-squares fit with two floating parameters for the $k_1(T)$ data set using an equation of the form $k_1(T) = AT^n$ yields the recommended expression

$$k_1(T) = (1.85 \times 10^{-9})T^{-0.66}\ \mathrm{cm^3\,molecule^{-1}\,s^{-1}} \quad (297-766\ \mathrm{K}) \quad \text{(III)}$$

for the rate coefficient temperature dependence of the reaction OH with Br_2. (Numbers in parentheses indicate the temperature range.) 2σ error limits of the parameters A and n in expression III are 3.2×10^{-10} cm^3 molecule^{-1} s^{-1} and 0.03, respectively. The maximum and the average square deviations of our experimental rate coefficients are only 3.4% and 1.8% of the calculated values; thus expression III reproduces our experimental data set of the measured rate coefficients very well.

To determine the limits of uncertainties of the measured k_1 values we subdivided sources of error in the measured experimental physical parameters into statistical and systematic categories according to their physical nature or behavior observed during the performance of the calibrations and experiments.[10] The evaluation of potential systematic errors was mainly based on the finite accuracies stated by the manufacturers for the devices used in our experiments. The uncertainties in the measured experimental parameters were propagated to the final values of the uncertainties in the measured rate coefficients, using different mathematical procedures for propagating systematic and statistical uncertainties.[20] The error limits of the experimentally determined rate coefficients listed in Table 1 represent the 2σ level of statistical (random) uncertainty only.

TABLE 2: Energies of Reactants, Products, and Stationary Points on the PES of the OH + Br_2 Reaction Obtained in Quantum Chemical Calculations[a]

	species[b]		
method	OH···Br_2	TS[b]	HOBr + Br
BH&HLYP/aug-cc-pVDZ optimization			
BH&HLYP/aug-cc-pVDZ	−7.41	9.78	−7.55
CCSD(T)/aug-cc-pVDZ	−10.08	−12.57	−36.70
CCSD(T)/aug-cc-pVTZ	−8.94	−10.32	−22.83
CCSD/aug-cc-pVDZ optimization			
CCSD/aug-cc-pVDZ	−8.91	4.36	−33.18
CCSD(T)/aug-cc-pVDZ	−10.29	−5.48	−37.47
CCSD(T)/aug-cc-pVTZ	−9.25	−4.86	−23.61
experimental[c]			−13.3 ± 8.8

[a] Energy values are given in kJ mol^{-1} relative to OH + Br_2 and include zero-point vibrational energy (ZPE) and spin−orbit corrections for OH (−0.000317 Hz) and Br (−0.005597 Hz). [b] PES saddle point between the OH···Br_2 complex and the HOBr + Br products. [c] Thermochemical data from refs 27−33.

The evaluated maximum of the systematic uncertainty in the experimental rate coefficients is 5% of the value. (See ref 10 for details.)

III. Potential Energy Surface and Transition State Theory Model of the OH + Br_2 Reaction

The potential energy surface (PES) of reaction 1 was studied by using quantum chemistry. Two methods were used for optimization of molecular structures and calculation of vibrational frequencies: density functional BH&HLYP[21,22] and CCSD,[23,24] both with the aug-cc-pVDZ basis set.[25] The Gaussian 03 program[26] was used in all potential energy surface (PES) calculations. The version of the BH&HLYP functional implemented in Gaussian 03[26] was used which, as described in the Gaussian manual, is different from that of ref 21. In addition, high-level single-point energy calculations were carried out for the PES stationary points by using the CCSD(T)[23,24] method with two basis sets, aug-cc-pVDZ and aug-cc-pVTZ.[25] All CCSD(T) results lead to the same qualitative conclusions regarding the mechanism of reaction 1; energy values quoted in the text henceforth are those obtained in the CCSD(T)/aug-cc-pVTZ//CCSD/aug-cc-pVDZ calculations and include vibrational zero- point energies unless stated otherwise. The results of the PES study are summarized in Table 2 and the detailed information is given in the Supporting Information (Table 1S, Figure 1S).

The reaction path leading from the OH + Br_2 reactants to the HOBr + Br products has a shallow van der Waals minimum (weakly bound OH···Br_2 complex, −9.2 kJ mol^{-1} relative to the reactants) on the reactants side, followed by a small energy barrier (PES saddle point, −4.9 kJ mol^{-1} relative to the reactants). In this respect, the mechanism of reaction 1 is qualitatively similar to that of the reaction between OH and Cl_2.[10] However, the top of the energy barrier is below the energy of the reactants, unlike in the case of the OH + Cl_2 reaction, where the barrier is located ∼10 kJ mol^{-1} above the reactants.

In an attempt to provide the means for an extrapolation of the experimental $k_1(T)$ dependence to temperatures outside the experimental range, an RRKM model of reaction 1 was created in the current work. Molecular structure and vibrational frequencies of the saddle point obtained in the CCSD/aug-cc-pVDZ-level calculations were used, together with the experimental properties of the reactants and products.[27−33]

Modeling was performed under the assumption that most of the trajectories sampling the coordinate space of the OH···Br_2

complex and having energies above that of the reactants proceed back to OH + Br_2 and only a small fraction pass through the PES saddle point and lead to the HOBr + Br products. Thus, the saddle point was assumed to represent the dynamic bottleneck of the reaction. This is a reasonable assumption given the fact that the decomposition of the OH···Br_2 complex back to the reactants is expected to have a transition state that is significantly "looser" and thus has larger density of states than that of the OH···Br_2 → HOBr + Br route.

Rate coefficient values were calculated by using the equation

$$k(T) = \frac{Q^{\ddagger}_{trans}(T)Q^{\ddagger}_{inact}(T)}{hQ_{OH}(T)Q_{Br_2}(T)}\int_{E_0}^{\infty} W^{\ddagger}(E - E_1)\exp\left(-\frac{E-E_0}{k_B T}\right)\mathrm{d}E \quad \text{(IV)}$$

where $Q^{\ddagger}_{trans}(T)$ and $Q^{\ddagger}_{inact}(T)$ are the partition functions of the translational and the overall 2-dimensional (inactive) rotational degrees of freedom of the transition state, $Q_{OH}(T)$ and $Q_{Br_2}(T)$ are the partition functions of the OH and Br_2 reactants, $W^{\ddagger}(E - E_1)$ is the sum-of-states function of the active[34−36] degrees of freedom of the transition state, E_0 and E_1 are the energies of the reactants and the transition state, respectively ($E_0 > E_1$), and k_B and h are the Boltzmann and the Planck constants. Equation IV was obtained by simplification of a formula derived by Mozurkewich and Benson[37] (eq 12 of ref 37) for reactions proceeding over shallow potential energy wells. The simplification resulted from the above-mentioned assumption of predominant dissociation of the OH···Br_2 complexes to OH + Br_2 and from an approximate treatment of the effects of angular momentum (J) conservation where the rate coefficient value obtained for $J = 0$ is multiplied by the ratio of the partition functions of the two-dimensional rotational (inactive) degrees of freedom of the transition state and the active molecule. The latter ratio (1.2) is close to unity, which justifies the use of the approximation.

The reaction transition state has one torsional degree of freedom. The PES of this torsion, obtained by using a BH&HLYP relaxed scan of the H−O−Br−Br dihedral angle, has two unequal maxima (5 and 30 kJ mol^{-1}). The partition function of this torsional degree of freedom was calculated by summing over the energy levels evaluated via a numerical solution of the Schrödinger equation. The FGH1D program[38] of Johnson was used in the energy level calculations. For the calculation of the sum-of-states function ($W^{\ddagger}(E - E_1)$), this degree of freedom was replaced with a sinusoidal internal hindered rotor with the rotational constant $B = 29.5$ cm^{-1} and the hindering barrier height of 10.1 kJ mol^{-1}. These parameters were selected so that the temperature dependence of the resultant partition function matched that obtained by using the exact energy levels with the accuracy of 3% or better in the 200−3000 K temperature range. Existence of the low-lying excited electronic state[27] of OH (139.7 cm^{-1}) was taken into account in the rate coefficient calculations.

The rate coefficients calculated with use of the saddle point (transition state) energy of −4.9 kJ mol^{-1} relative to the reactants obtained in the CCSD(T)/aug-cc-pVTZ//CCSD/aug-cc-pVDZ calculations are presented in Figure 3 (red dotted line). The calculated rate coefficients are, on average, 40% lower that the experimental values. Adjustment of the saddle point energy by −2 kJ mol^{-1} (to −6.9 kJ mol^{-1}) results in a better average agreement with experiment (red dashed line). However, despite the general agreement with the experimental temperature dependence of the rate coefficient of reaction 1, the calculated $k_1(T)$ line displays a markedly different trend in its curvature on an Arrhenius plot. While our experimental data set has a slight negative curvature, the results of modeling exhibit a slight positive curvature.

IV. Comparison with Previous Studies and Discussion

To our knowledge, all previous direct kinetic studies[5−9] of the reaction of OH + Br_2 have been performed at low temperatures. Data reported in refs 5 and 6 were measured at room temperature only. The rate coefficient value obtained by Poulet et al.[5] is in excellent agreement with that given by expression III at room temperature. The resulting k_1 value reported by Loewenstein et al.[6] is 23% higher than that given by expression III at room temperature. Nevertheless, it agrees with our room-temperature measurement within combined experimental uncertainties of both studies.

Experimental temperature-dependent kinetic investigations of the reaction of the hydroxyl radical with molecular bromine were carried out in three studies.[7−9] Boodaghians et al.[7] measured k_1 at four temperatures only over the temperature range of 262−303 K. As can be seen from Figure 3 these k_1 data are systematically lower than ours and those from refs 5−9 in the common temperature intervals, but they are in agreement with them near room temperature within the experimental uncertainties. Their data show a slight positive temperature dependence (see Figure 3). However, Boodaghians et al.[7] preferred to regard the reaction of OH with Br_2 as being temperature independent within experimental uncertainty over the temperature range studied.

Measurements performed in refs 8 and 9 showed distinct, albeit weak, negative temperature dependences $k_1(T) = (1.98 \pm 0.51) \times 10^{-11}\exp[(238 \pm 70\ \mathrm{K}/T)]$ and $(1.8 \pm 0.3) \times 10^{-11}\exp[(235 \pm 50\ \mathrm{K}/T)]$ cm^3 $molecule^{-1}$ s^{-1}, respectively, which are in agreement with each other. As can be seen from Figure 3 the plot of eq III lies between the data obtained by Gilles et al.[8] and Bedjanian et al.[9] These data are in agreement with eq III within the reported experimental uncertainties and can be combined with the current experimental $k_1(T)$ data set. Indeed, if our $k_1(T)$ data set is combined with the $k_1(T)$ data sets from refs 8 and 9, then the least-squares fit of the resultant combined set of data to the equation of the form $k_1(T) = AT^n$ yields the expression

$$k_1(T) = (1.96 \times 10^{-9})T^{-0.67}\ \mathrm{cm^3\,molecule^{-1}\,s^{-1}} \quad (230 - 766\ \mathrm{K}) \quad \text{(V)}$$

The maximum and average square deviations of experimental rate coefficient values of the resultant combined set of data from those calculated by using two-parameter expression V are 15% and 6% of the calculated value, respectively. The maximum deviation between values given by eqs III and V is 0.9% in the temperature range 230−766 K. Thus, either expression III or V can be recommended for the temperature dependence of the reaction of the hydroxyl radical with molecular bromine in the temperature range from 230 to 766 K, because these two expressions give practically the same values of $k_1(T)$.

HOBr and Br are expected to be the products of reaction 1. This product channel is exothermic ($\Delta H^0_{298} = -15.7 \pm 8.8$ kJ mol^{-1} [27−29]). The only other product channel that can be suggested, that producing HBr + BrO, is endothermic ($\Delta H^0_{298} = 14.8 \pm 6.4$ kJ mol^{-1} [27,28,30]). A 100% yield of the atomic Br product was observed in reaction 1 experimentally.[5,6] The conclusion of the dominance of the HOBr + Br product channel is also supported by an analogy with the OH + Cl_2 reaction where a 100% yield of Cl was observed experimentally[6] and a

PES study performed in ref 10 demonstrated that the reaction proceeds to form only HOCl + Cl products, with the alternative (HCl + ClO) channel requiring overcoming a large potential energy barrier.

The rate coefficients calculated by using the model of reaction 1 created in the current study on the basis of CCSD(T)/aug-cc-pVTZ//CCSD/aug-cc-pVDZ PES calculations are, generally, in good agreement with the experimental values. Without any model adjustment, the calculated rate coefficient values are only ~40% lower than the experimental ones. This deviation is quite reasonable for a model completely based on ab initio PES. Adjustment of the energy of the PES saddle point by only −2 kJ mol^{-1} brings the calculated values into a much better agreement with experiment. Comparison of the experimental and the calculated 0 K enthalpies of reaction 1 (Table 2) is not very conclusive regarding the adequacy of the computational methods used because of the large uncertainty of the experimental value resulting, primarily, from that in the $\Delta H_f^0{}_{298}$(HOBr) (±8.4 kJ mol^{-1});[29] the 0 K reaction enthalpy values calculated at the CCSD(T)/aug-cc-pVTZ level are only 0.7−1.4 kJ mol^{-1} outside of the estimated envelope of uncertainty of the experimental value. The deviation depends on the size of the basis set used in single-point energy calculations: it becomes significantly larger (~15 kJ mol^{-1}) if the smaller aug-cc-pVDZ basis set is used.

Despite the generally good agreement between the calculated and the experimental values of the rate coefficients, the failure of the computational model to reproduce the experimental negative curvature of the Arrhenius plot of the rate coefficient is disconcerting. The model thus is not suitable for extrapolation of the experimental data to temperatures outside the experimental range. Instead, use of eq III or V is recommended. It may be possible that a more involved version of the rate theory (e.g., microcanonical variational approach to the selection of the position of the dynamic bottleneck of the reaction and explicit accounting for the finite ratio of the rates of dissociation of the OH···Br_2 complex to reactants and products) can improve the agreement between computations and experiment. However, application of more complicated versions of rate theory will be meaningful only if a larger degree of certainty is achieved in the properties of the reaction PES.

Acknowledgment. This research was supported by the Patrick F. Taylor Chair Foundation. The authors would like to thank Dr. J. N. Crowley, Dr. J. Hogan, and Mr. S. Bagley for helpful discussion and advice. This study utilized the high-performance computational capabilities of the Biowulf PC/Linux cluster at the National Institutes of Health, Bethesda, MD (http://biowulf.nih.gov).

Supporting Information Available: Results of the quantum chemical calculations and the reaction potential energy surface diagram (Table 1S and Figure 1S). This material is available free of charge via the Internet at http://pubs.acs.org.

References and Notes

(1) Soderstrom, G.; Marklund, S. *Environ. Sci. Technol.* **2002**, *36*, 1959.
(2) Evans, C. S.; Dellinger, B. *Environ. Sci. Technol.* **2003**, *37*, 5574.
(3) Soderstrom, G.; Marklund, S. *Environ. Sci. Technol.* **2004**, *38*, 825.
(4) Evans, C. S.; Dellinger, B. *Environ. Sci. Technol.* **2005**, *39*, 2428.
(5) Poulet, G.; Laverdet, G.; Le Bras, G. *Chem. Phys. Lett.* **1983**, *94*, 129.
(6) Loewenstein, L. M.; Anderson, J. G. *J. Phys. Chem.* **1984**, *88*, 6277.
(7) Boodaghians, R. B.; Hall, I. W.; Wayne, R. P. *J. Chem. Soc., Faraday Trans. 2* **1987**, *83*, 529.
(8) Gilles, M. K.; Burkholder, J. B., Ravishankara, A. R. *Int. J. Chem. Kinet.* **1999**, *31*, 417.
(9) Bedjanian, Y.; Le Bras, G.; Poulet, G. *Int. J. Chem. Kinet.* **1999**, *31*, 698.
(10) Bryukov, M. G.; Knyazev, V. D.; Lomnicki, S. M.; McFerrin, C. A.; Dellinger, B. *J. Phys. Chem. A* **2004**, *108*, 10464.
(11) Droege, A. T.; Tully, F. P. *J. Phys. Chem.* **1986**, *90*, 1949.
(12) Atkinson, R.; Baulch, D. L.; Cox, R. A.; Hampson, R. F., Jr.; Kerr, J. A.; Rossi, M. J.; Troe, J. *J. Phys. Chem. Ref. Data* **1997**, *26*, 1329.
(13) Wollenhaupt, M.; Carl, S. A.; Horowitz, A.; Crowley, J. N. *J. Phys. Chem. A* **2000**, *104*, 2695.
(14) D′Ottone, L.; Campuzano-Jost, P.; Bauer, D.; Hynes, A. J. *J. Phys. Chem. A* **2001**,*105*, 10538.
(15) Silvente, E.; Richter, A. C.; Hynes, A. J. *J. Chem. Soc., Faraday Trans.* **1997**, *93*, 2821.
(16) Tully, F. P.; Golgsmith, J. E. M. *Chem. Phys. Lett.* **1985**, *116*, 345.
(17) Tully, F. P.; Droege, A. T.; Koszykowski, M. L.; Melius, C. F. *J. Chem. Phys.* **1986**, *90*, 691.
(18) Orkin, V. L.; Huie, R. E.; Kurylo, M. J. *J. Phys. Chem.* **1996**, *100*, 8907.
(19) Kurylo, M. J.; Orkin, V. L. *Chem. Rev.* **2003**, *103*, 5049.
(20) Bevington, P. R. *Data Reduction and Error Analysis for the Physical Sciences*; McGraw-Hill: New York, 1969.
(21) Becke, A. D. *J. Chem. Phys.* **1993**, *98*, 1372.
(22) Lee, C. T.; Yang, W. T.; Parr, R. G. *Phys. Rev. B* **1988**, *37*, 785.
(23) Cizek, J. *Adv. Chem. Phys.* **1969**, *14*, 35−89.
(24) Purvis, G. D. I.; Bartlett, R. J. *J. Chem. Phys.* **1982**, *76*, 1910.
(25) Kendall, R. A.; Dunning, T. H., Jr.; Harrison, R. J. *J. Chem. Phys.* **1992**, *96*, 6796.
(26) Frisch, M. J.; Trucks, G. W.; Schlegel, H. B.; Scuseria, G. E.; Robb, M. A.; Cheeseman, J. R.; Montgomery, J. A., Jr.; Vreven, T.; Kudin, K. N.; Burant, J. C.; Millam, J. M.; Iyengar, S. S.; Tomasi, J.; Barone, V.; Mennucci, B.; Cossi, M.; Scalmani, G.; Rega, N.; Petersson, G. A.; Nakatsuji, H.; Hada, M.; Ehara, M.; Toyota, K.; Fukuda, R.; Hasegawa, J.; Ishida, M.; Nakajima, T.; Honda, Y.; Kitao, O.; Nakai, H.; Klene, M.; Li, X.; Knox, J. E.; Hratchian, H. P.; Cross, J. B.; Bakken, V.; Adamo, C.; Jaramillo, J.; Gomperts, R.; Stratmann, R. E.; Yazyev, O.; Austin, A. J.; Cammi, R.; Pomelli, C.; Ochterski, J. W.; Ayala, P. Y.; Morokuma, K.; Voth, G. A.; Salvador, P.; Dannenberg, J. J.; Zakrzewski, V. G.; Dapprich, S.; Daniels, A. D.; Strain, M. C.; Farkas, O.; Malick, D. K.; Rabuck, A. D.; Raghavachari, K.; Foresman, J. B.; Ortiz, J. V.; Cui, Q.; Baboul, A. G.; Clifford, S.; Cioslowski, J.; Stefanov, B. B.; Liu, G.; Liashenko, A.; Piskorz, P.; Komaromi, I.; Martin, R. L.; Fox, D. J.; Keith, T.; Al-Laham, M. A.; Peng, C. Y.; Nanayakkara, A.; Challacombe, M.; Gill, P. M. W.; Johnson, B.; Chen, W.; Wong, M. W.; Gonzalez, C.; Pople, J. A. *Gaussian 03*, Revision C.02; Gaussian, Inc.: Wallingford, CT, 2004.
(27) Chase, M. W., Jr. *J. Phys. Chem. Ref. Data* **1998**, *Monogr. 9*, 1−1951.
(28) Ruscic, B.; Wagner, A. F.; Harding, L. B.; Asher, R. L.; Feller, D.; Dixon, D. A.; Peterson, K. A.; Song, Y.; Qian, X. M.; Ng, C. Y.; Liu, J. B.; Chen, W. W. *J. Phys. Chem. A* **2002**, *106*, 2727.
(29) Orlando, J. J.; Tyndall, G. S. *J. Phys. Chem.* **1996**, *100* (50), 19398.
(30) Bedjanian, Y.; LeBras, G.; Poulet, G. *Chem. Phys. Lett.* **1997**, *266*, 233.
(31) Koga, Y.; Takeo, H.; Kondo, S.; Sugie, M.; Matsumura, C.; McRae, G. A.; Cohen, E. A. *J. Mol. Spectrosc.* **1989**, *138*, 467.
(32) McRae, G. A.; Cohen, E. A. *J. Mol. Spectrosc.* **1990**, *139*, 369.
(33) Cohen, E. A.; McRae, G. A.; Tan, T. L.; Friedl, R. R.; Johns, J. W. C.; Noel, M. *J. Mol. Spectrosc.* **1995**, *173*, 55.
(34) Robinson, P. J.; Holbrook, K. A. *Unimolecular Reactions*; Wiley-Interscience: New York, 1972.
(35) Gilbert, R. G.; Smith, S. C. *Theory of Unimolecular and Recombination Reactions*; Blackwell: Oxford, UK, 1990.
(36) Holbrook, K. A.; Pilling, M. J.; Robertson, S. H. *Unimolecular Reactions*, 2nd ed. Wiley: New York, 1996.
(37) Mozurkewich, M.; Benson, S. W. *J. Phys. Chem.* **1984**, *88*, 6429.
(38) Johnson, R. D. I. *FGH1D* [PC/Windows program for computing vibrational levels for nonharmonic potentials]; National Institute of Standards and Technology: Gaithersburg, MD 20899.